UNDERWATER LINEAR FEATURE EXTRACTION WITH MULTISPECTRAL BAND IMAGES: AN EVALUATION WITH LEVEL-SET METHOD IN DONGSHA ATOLL AND ZENGMU SHOAL

Peter Tian-Yuan Shih[1], Jian-Wei Lin[1], Wei-Tsun Lin[1], and Cheng-Gi Wang[2]

ABSTRACT

Optical remote sensing satellite images are a useful and convenient source to provide underwater features, particularly for shallow water areas because light, dependent on wavelength, has the capability to penetrate water. In this study, the information richness of underwater features is investigated for each spectral band of the optical images, and also several derived bands. This assessment is performed with the level-set method for segmentation.

Two cases are analyzed in this study. The first study site is the Dongsha atoll, which is composed of Dongsha island, lagoon, and surrounding reefs. The water depth ranges from zero to less than 3 m at the outer ring and down to a depth of 20 m in the lagoon. The images were acquired with WorldView-2 in October 2013 and covered the entire atoll. The second study site is Zengmu shoal, an underwater feature. The image used is a scene acquired with Landsat 8. These images demonstrate high water clarity in both sites.

For the Dongsha atoll, both the reflectance of each spectral band, the NDWI, and bands processed with Principle Component Transformation (PCT) are analyzed. The assessment is made based on the number of segments identified. The more segments identified, subsequently the more information, we assume, is provided. In order to remove those caused by noise, only the segments larger than 100 m^2 were counted. Based on this, PCT band 1 performs the best, and followed by green, yellow, coastal, blue, red, and fewer features from red-edge NIR and NIR2 bands when the objects in the scene are completely submerged underwater. For the Zengmu shoal, the boundary of the object identified is used for the assessment. The one closest to the manually digitized imaged boundary would be recognized as having the best performance. Among the spectral bands, coastal/aerosol (CA) and blue perform the best. The four bands, coastal, blue, green, and red, are projected with PCT. The boundary resulting from the first principle component resembles most the one identified by a human operator on a QuickBird image.

I. INTRODUCTION

The multispectral images from sensors onboard the satellite have been applied to numerous studies on a wide variety of environmental phenomena, such as water quality (Hellweger, et al., 2004), chlorophyll detection (Giardino et al., 2001; Palmer et al., 2015), underwater light climate (Liu et al., 2010), and shallow water bathymetry (Pacheco et al., 2015), to name a few. In addition these images are also popularly applied to benthic habitat mapping (Reshitnyk et al., 2014).

While the Enhanced Thematic Mapper Plus (ETM+) onboard Landsat 7 has seven multispectral bands, the Operational Land Imager (OLI) onboard Landsat 8 has ten. In the visible region, OLI has a coastal/aerosol band with a spectral range of 0.433-0.453 μm in addition to the blue, green and red bands. The principle objective of adding this band is for ocean color observations in coastal zones (Irons et al., 2012), which can be used for the characterization of aerosol optical properties in removing atmospheric effects over land targets. This band is, therefore, referred to as the coastal/aerosol (CA) band (Pahlevan et al., 2014). Landsat 8 was launched on Feb. 11, 2013. The World-View-2 (WV-2) launched in 2009 also carries two bands other than R, G, B, namely, the coastal band (0.400-0.450 μm) and yellow band (0.585-0.625 μm). The availability of the World-View-2 coastal band and Landsat CA band allowed immediate application for a number of water related studies, such as, Marcello et al. (2015) that utilized a WV-2 image to analyze a submarine volcanic eruption; Reshitnyk et al. (2014) where procedures for mapping the distribution of submerged aquatic vegetation at a site within the Gwaii Haanas National Marine Conservation Area off the north coast of British Columbia, Canada were evaluated; Vahtmaee and Kutser (2013) who experimented

Table 1. The Spectral Bands of WorldView-2 (Updike & Comp, 2010).

Band	Wavelength Range (nm)	Center Wavelength (nm)
Coastal	401.4-453.2	427.0
Blue	447.5-508.3	478.3
Green	511.3-581.1	545.8
Yellow	588.5-627.0	607.7
Red	629.2-688.5	658.8
RedEdge	703.8-743.6	724.1
NIR1	772.4-890.2	832.9
NIR2	861.7-954.2	949.3
Panchromatic	463.7-800.6	627.4

Table 2. The Spectral Bands of OLI (Irons & Masek, 2006).

Band	Wavelength (nm)	Center Wavelength (nm)
Coastal/Aerosol	0.43-0.45	443
Blue	0.45-0.51	482
Green	0.53-0.59	562
Red	0.64-0.67	655
NIR	0.85-0.88	865
SWIR 1	1.57-1.65	1610
Cirrus	1.36-1.38	1372
SWIR-1	2.11-2.29	2200
TIRS 1	10.60-11.19	10800
TIRS 2	11.50-12.51	12000
Panchromatic	0.50-0.68	590

with classifying the Baltic Sea shallow water habitats. Although all of these studies use multiple data sources, the contribution of WV-2 images is significant. This is clear as other data sources used in Pacheco et al. (2015) utilized the CA, blue, and green bands of Landsat 8 OLI for shallow water bathymetric mapping. Likewise, Vanhellemont and Ruddick (2015) studied the spatial distribution of marine and atmospheric features of turbid Belgian coastal waters with Landsat 8 images.

The objective of this study is to evaluate how informative the multispectral images are for benthic object identification. The scheme adopted is to segment the image with the level set method. Then, the result is assessed in two ways. In the first scenario, the number of objects identified is used as a measure, since there are many objects in the scene. The alternative compares the boundary extracted with level set and the one manually digitized. The discrepancy is measured with point-to-line deviations.

II. THE LEVEL SET METHOD

The level-set method was originally introduced by Osher and Sethian (1988) and has been developed into one of the most useful tools for segmentation. Level-set method utilizes initial curve, which is an iso-contour. This initial curve, dependent on image energy, is considered to be the zero level set function or baseline value. During the process of analysis, the initial curve is gradually moving to the minimum of image energy and the final curve then becomes the area boundary. Mumford and Shah (1989) proposed an energy equation to find the minimum image energy and assumed that images are composed of limited sub-regions and regional boundaries. Vese and Chan (2002) utilized the energy equation proposed by Mumford and Shah (1989) and assumed that the regional color code is the average number of pixel values both from the inside and outside of the regional boundary. The new energy equation proposed by Vese and Chan (2002) utilized a least-squares function to find the minimum of the energy equation. Level-set function regularized Heaviside function (unit-step function) to determine whether the pixel is in or out of the boundary. When the pixel is inside the boundary, the Heaviside function is equal to 1. Therefore, while the initial

curve is zero, this curve is the regional boundary. We can minimize the energy function by adjusting the regional color code. Huang and Wu (2010), Huang and Huang (2011) and Huang et al. (2014) applied Level-set to image segmentation with different types of images, extracting various features. The same algorithm and implementation is applied in this study, with a detailed parameterization of equations referred to in these three articles.

III. THE EXPERIMENTS

Two cases are analyzed: the first being the Dongsha atoll located in the east portion of the South China Sea, which is composed of Dongsha island, lagoon, and surrounding reefs. The water depth ranges from zero to less than 3 m at the outer ring and 20 m in the lagoon. In October of 2013, two image scenes were acquired with WorldView-2 that span the entire atoll. The image process level is standard 2a, and the spatial resolutions of the panchromatic and multispectral images are 0.5 m and 2 m, respectively. The multispectral image has eight channels, including coastal, blue, green, yellow, red, red-edge, NIR1 and NIR2. The range and center for wavelengths in each band are listed in Table 1.

The second study site is the Zengmu shoal, also located in the South China Sea, but in the Southern end, and is completely an underwater feature. The image used is a scene acquired with Landsat 8 OLI. The wavelength range and center of each spectral band are shown in Table 2. In the WRS, it is identified as path 120, row 57. The image process level is 1T, with data downloaded from EarthExplorer (http://earthexplorer.usgs.gov/). The goal of this case is to identify the boundaries of the Zengmu shoal. The level set method is applied to CA, blue, green, and red bands.
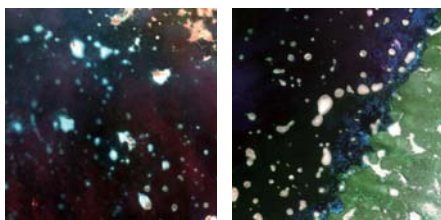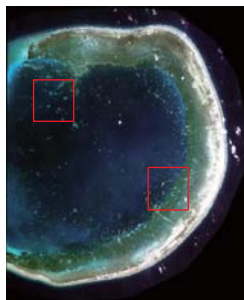
1. Dongsha Atoll

With the WorldView-2 images, atmospheric correction was performed first to derive the reflectance of each band. The eight multispectral bands and the panchromatic band were analyzed.

Table 3. The Depth of the Test Area (m).

	Area 1	Area 2
Max. depth	23.93	17.54
Min. depth	1.30	0.47
Mean depth	12.10	9.30
St. deviation	3.46	5.34

Table 4. The Number of Segments, Dongsha.

| Band	Area 1	Area 2	Derived Band	Area 1	Area 2
Coastal	23	51	NDWI	34	56
Blue	20	61	$NDWI_{WV2}$	27	37
Green	42	76	PCT-B1	47	63
Yellow	38	78	PCT-B2	53	48
Red	7	81			
RedEdge	5	68			
NIR	1	60			
NIR2	1	14			

Fig. 1. The Study Area of Dongsha Atoll (Left, area 1; Right: area 2).

Two sub-scenes were extracted from the image 052901328070_ 01_P002. As shown in Fig. 3, area 1 is mainly located inside the lagoon; while area 2 is located at the edge of the reef. Geographically, the upper-left corner of the bounding box of these two areas are, area 1 (20°4'3.41N; 116°6'40.69E), area 2 (20°0'32.54N; 116°1'40.26E). The dimensions of both sub-scenes are 1500 × 1500 pixels. The results are shown in Figs. 2 and 3 for areas 1 and 2, respectively.

In both areas 1 and 2, the terrain features are all underwater (Table 3). However, area 2 is relatively shallower than area 1. As shown in Fig. 1, the East-South portion of area 1 is located on the reef flat. The depth of the flat is generally below one meter. Considering the tide effect, it is very likely that some of the reef flat was covered by a few centimeters of water at the time of imaging.

Band	Segmentation	Band	Segmentation
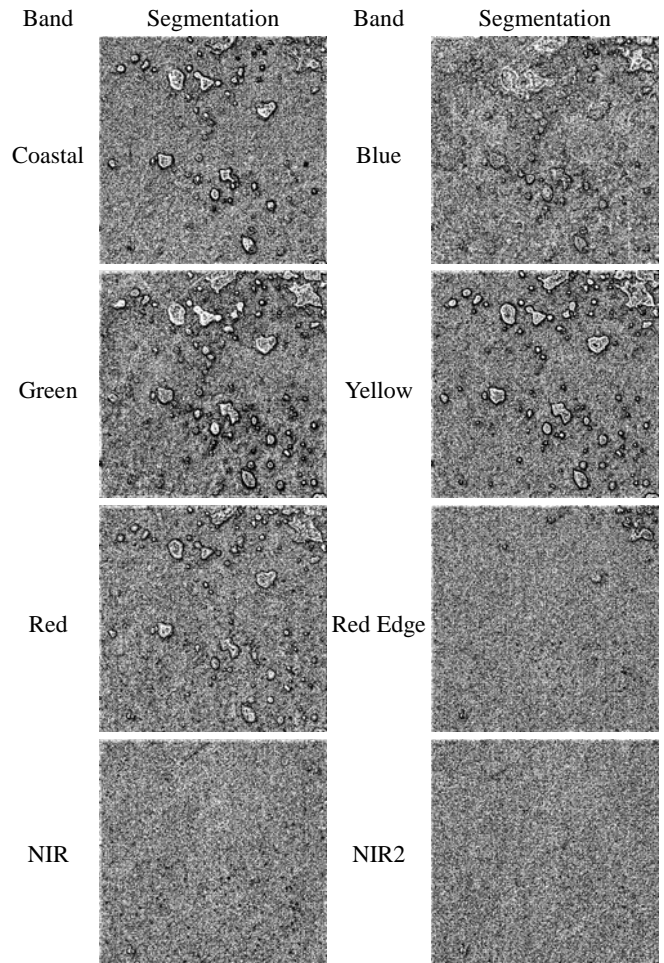
Fig. 2(a). The Segmentation with Original Bands, Area 1.
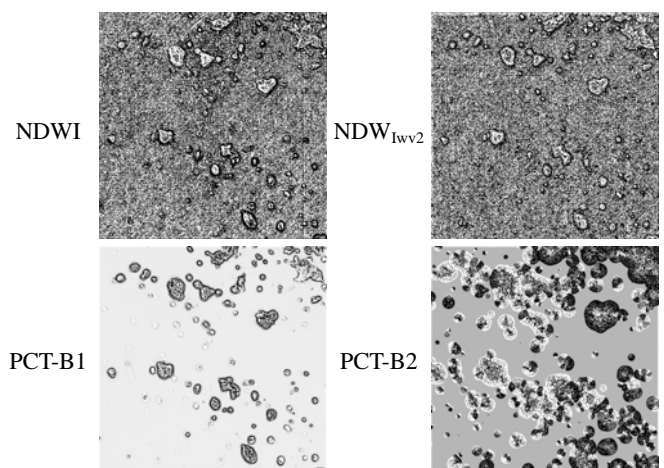
Fig. 2(b). The Segmentation with Derived Bands, Area 1.

The assessment is performed by counting the number of segments identified. Bands with a high number of identified segments are considered to have rich information content. In order to avoid influence from noises, only those segments
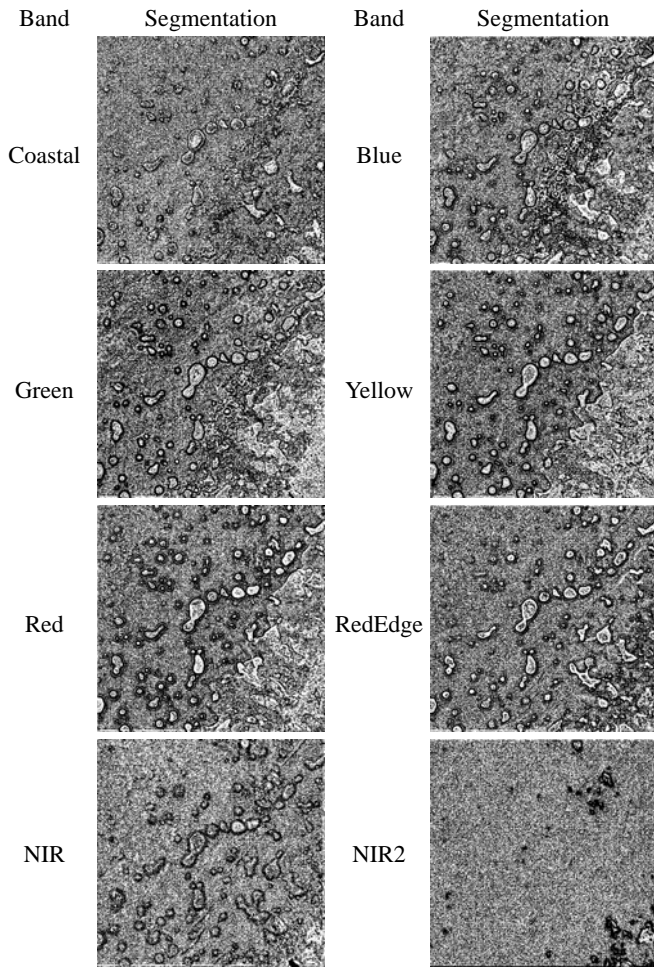
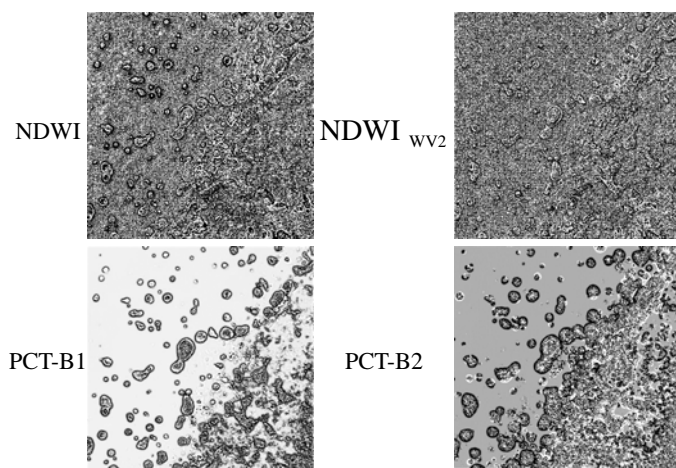Fig. 3(a). The Segmentation with Original Bands, Area 2.

Fig. 3(b). The Segmentation with Derived Bands, Area 2.

Fig. 4. Zengmu Shoal, Landsat 8.

the red, red-edge, NIR and NIR2 bands, the coastal, blue and green bands provide more segments. NDWI (Normalized Difference Water Index) originally proposed by McFeeters (1996) is formulated by taking the modulation of green and NIR bands. Wolf (2010) proposed an NDWI for WV-2 images by taking the modulation of coastal and NIR2 bands. This index has been applied in Maglione et al. (2014) for shoreline extraction, and proved as better than NDVI for this application. The NDWI formed with two band combinations are applied to the Dongsha Atoll analysis. The result shows that NDWI is more informative for extracting underwater objects.

$$\text{NDWI} = \frac{(\text{Green} - \text{NIR})}{(\text{Green} + \text{NIR})}$$

$$\text{NDWI}_{\text{WV2}} = \frac{(\text{Coastal} - \text{NIR2})}{(\text{Coastal} + \text{NIR2})}$$

As delineated in Table 4, in terms of the features identified, the red band performed the best among all bands in area 2. This area is largely an underwater feature with an average depth of 12.10 m. The depth of this area ranges between 1.3 to 23.93 m. One third of area 2 is located on the reef flat of the atoll. At the time of the satellite imaging, the reef was covered by a very thin layer of water. This explains why the yellow band performs the best in this area, and both red and red-edge also performs well. Notably, the Coastal band does not identify more features in both areas.

2. Zengmu Shoal

From the Landsat 8 image LC81200572014114LGN00, acquired on 2014-04-24, a sub-scene of Zengmu shoal is extracted. The dimension of this sub-scene is 122 x 106. The four bands which have better water penetration capability, CA, blue, green, and red bands, are shown in Fig. 4. Principal Component

larger than or equal to 100 square meters are counted, as shown in Table 4. From the results of area 1, the coastal, blue, green, yellow, red, red-edge, NIR and NIR2 bands have 23, 20, 42, 38, 7, 5, 1 and 1 segments, respectively. Compared with
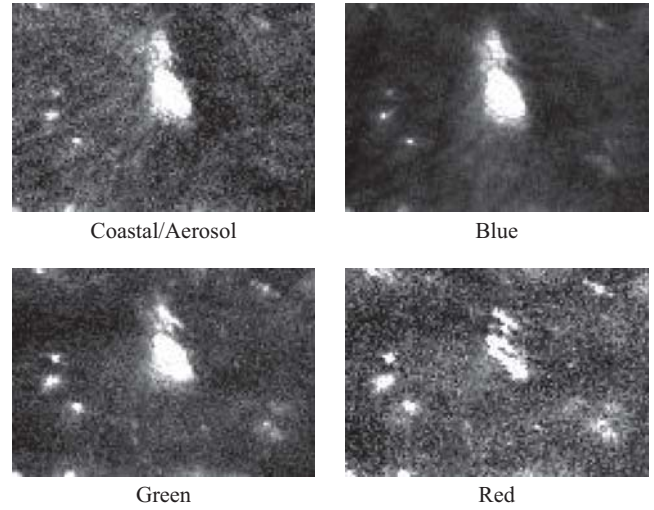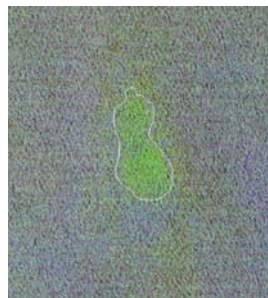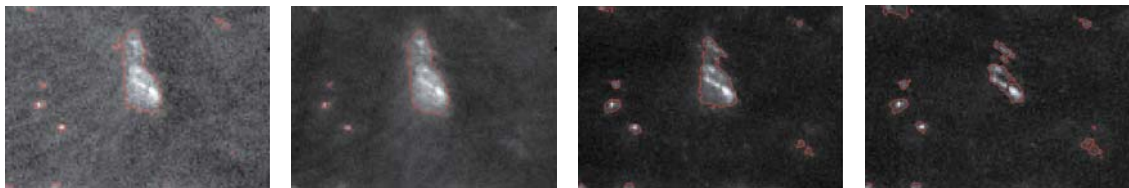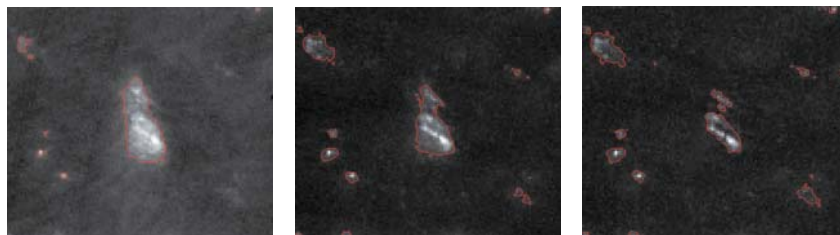
Fig. 5. The Principle Components (Left to right: PCT-B1 to PCT-B3).

(a) The Manually Digitized

(b) The CA, Blue, Green (first line) and Red (second line)

(c) The First, Second, Third, Components (from left to right)

Fig. 6. Zengmu Shoal, Landsat 8 Boundaries and Segments.

Transformation (Richards, 2013) is applied to these four bands, as shown in Fig. 5. Aside from the NDWI and the NDWI$_{CA}$, an index replaced green band in NDWI equation with CA band are also included. Then, these nine images are processed with the level set method.

Unlike the Dongsha Atoll situation, where there are many features with different scales, the Zengmu Shoal has only one specific feature under study. When the scale parameter is smaller than 15, the resulting segments are quite fragmented. However, for those with scale parameter 15 and above, the result is about the same. Therefore, the segments from scale parameter 15

are applied for the analysis. As shown in Fig. 6, while the CA, blue, and green share large similarities, red has larger differences, although each presents differently for the principal components. Among the three components, the segment from the first most resembles the one digitized manually.

For the evaluation, a manually digitized scene of a QuickBird-2 image acquired in 2009 as the backdrop is available from Hsu et al. (2015) as a reference boundary. This boundary line is shown in Fig. 6(a). All the boundaries are imported into ArcGIS 10.3 (ESRI, 2015) as different layers. Then, the deviations are analyzed with the near tool in the proximity toolset of the analysis

Table 5. The Distance Measure of Near Analysis, Zengmu Shoal.

(a) Reference to the Digitized Boundary

	Maximum	Minimum	Average	Standard Deviation	Total Points
CA	111.560	1.249	36.871	29.389	147
Blue	126.253	0.643	52.447	34.498	132
Green	191.854	1.250	73.276	52.744	140
NDWI	255.492	3.822	95.263	63.771	144
NDWI$_{CA}$	260.460	0.309	92.343	66.111	272
PCT-B1	110.648	0.786	42.887	26.483	135

(b) Reference to the 30 m Iso-Depth Line

	Maximum	Minimum	Average	Standard Deviation	Total Points
CA	104.829	0.134	20.993	19.273	147
Blue	88.406	0.178	18.901	15.950	132
Green	134.612	0.190	51.260	38.921	140
NDWI	225.601	1.772	53.107	53.107	144
NDWI$_{CA}$	228.922	1.352	53.681	53.681	272
PCT-B1	103.167	0.213	27.634	27.634	135
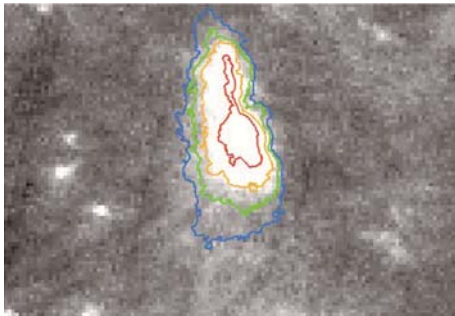
Fig. 7. Iso-Depth Lines of ZhengMu Shoal (Depth value from exterior, 40, 35, 30, and 25 m).

tool box (ESRI, 2010). The algorithm utilized in this tool takes one boundary as the line feature while the other is the point feature. The distance from all points on one boundary to the other boundary line is then computed. The statistical analysis of the deviations are delineated in Table 5(a).

Zengmu Shoal's different brightness as opposed to the surrounding sea increases its visibility to passing surface vessels. Zengmu Shoal is a tableland on the sea floor according to an onsite study conducted by the Ministry of the Interior. That is, the depth is relatively shallower and the relatively brighter color partly results from the biological coverage of this tableland by a wide range of coral. Therefore, a comparison of the feature identified from Landsat image with the iso-depth lines would provide another view of the image information content. As shown in Fig. 7, the feature boundary identified from the image brightness generally fits the 30m iso-depth line the best. The bathymetric information was obtained with a multi-beam sonar survey conducted in 2014. The statistics of the deviations are listed in Table 5(b).

Besides the evaluation by the "near" function, the area and perimeter of the polygons produced from the segmentation are also compared with those digitized and the 30 m iso-depth line. The statistics of the deviations are listed in Table 6.

As there is only one feature in the manually digitized boundary, red and the second and third components are not included in the analysis. The additional segments identified may be scattered shoals around Zengmu Shoal. This also supports the finding that automated image analysis schemes may identify more features than a human operator.

As observed from Tables 5 and 6, the segmentation results from blue band of Landsat 8 outperforms the others in the two evaluation schemes, as well as when referenced to both the digitized boundary and the 30 m iso-depth line.

IV. CONCLUDING REMARKS

The objective of this study is to evaluate the information content inherent in the multispectral images, particularly the new additional coastal bands, for benthic object identification. From the Dongsha atoll case, the WV-2 image is evaluated. The assessment is based on the presumption that the more segments identified means more information is provided. Compared with the red, red-edge, NIR and NIR2 bands, the coastal, blue and green bands provide more segments. The green band showed more features could be identified in the area mostly underwater. Additionally, the yellow band has shown promising results in the areas submerged by very shallow water. However, the features identified from the coastal band are sparse. The reason could be the relatively higher noise of this band. Notably, there are deviations among features identified in different bands. This indicates that multi-band would provide more

Table 6. The Perimeter and Area, Zengmu Shoal.

	Perimeter (m)	Area (m^2)	ΔArea (m^2) to the Digitized boundary	ΔArea (m^2) to the 30 m iso-depth line
Digitized from QuickBird2	486749	3117.774		
30 m iso-depth line	415968	4296.919		
CA	393300	3452.605	-93449	-22668
Blue	418603	3072.631	-68146	2635
Green	289094	3069.954	-197656	-126875
NDWI	151541	3457.832	-335208	-264427
NDWI$_{CA}$	142709	3214.049	-343849	-273068
PCT-B1	439389	3180.537	-47360	23421

information than any specific single band. The good performance of NDWI and PCA also support this observation. The influencing factors of the number of segments identified would be the nature of objects in the scene, the nature of observation (spectral characteristics of band), and the segmentation scheme. In this study, the level-set is selected as the standard scheme. With the same scene, the nature of spectral band or derived band is observed. However, because the reef patch has a three-dimensional structure, the shape of its contours may change at different depths. Since the penetration capability changes with wavelength and the spectral signature of objects changes as well, the linear feature identified in each band will also be different. In other words, the objects observed in each band may not be the same. In this study, the impact from this source is mitigated by following the procedure that only those segments larger than or equal to 100 square meters are counted.

From the Zengmu Shoal case, where only one feature is under investigation and Landsat 8 OLI image is evaluated, the blue band outperforms the others. In this case, even the first principal component performs better than other components, with clear results that lack the detail as the one derived from the blue band directly. This is largely due to the fact that there is only one specific feature. Besides, the performance of the red channel is significantly different from the Dongsha Atoll case. This is largely due to the depth of water to the object. Finally, it should be noted that the assessment conducted in this study is performed with the level-set method. Different segmentation schemes may produce different results.

ACKNOWLEDGEMENT

REFERENCES

ESRI (2010). Near Analysis, Proximity Toolset, Analysis Toolbox, ArcGIS resource center, http://help.arcgis.com/en/arcgisdesktop/10.0/help/index.html#/Near/00080000001q000000/, last accessed on 2015-06-03.

ESRI (2015). ArcGIS 10.3 and ArcGIS Pro Modernize GIS for Organizations and Enterprises, http://www.esri.com/esri-news/releases/15-1qtr/arcgis-10-3-and-arcgis-pro-modernize-gis-for-organizations-and-enterprises, last accessed on 2015-06-03.

Giardino, C., M. Pepe, P. A. Brivio, P. Ghezzi and E. Zilioli (2001). Detecting chlorophyll, secchi disk depth and surface temperature in a sub-alpine lake using landsat imagery. The Science of the Total Environment 268, 19-29.

Hellweger, F. L., P. Schlosser, U. Lall and J. K. Weissel (2004). Use of satellite imagery for water quality studies in new york harbor. Estuarine, Coastal and Shelf Science 61, 437-448.

Hsu, W. C., P. T. Y. Shih, F. J. Jao, C. C. Wang, H. L. Chen and J. K. Liu (2015). The Seasonal Analysis of Landsat Imagery for Zengmu Shoal Boundary Extraction, manuscripts in preparation.

Huang, Y. S. and J. W. Wu (2010). Infrared thermal image segmentations employing the multilayer level set method for non-destructive evaluation of layered structures. NDT&E International 43, 34-44.

Huang, Y. S. and Y. C. Huang (2011). Segmenting SAR satellite images with the multilayer level set approach. IEEE Journal of Selected Topics in Applied Earth Observations and Remote Sensing 4(3), 632-642.

Huang, Y. S., C. T. Chiu, M. G. Lee and S.Y. Lin (2014). Applying the multilayer level set approach to explore the thermal surface characteristics of hot mix asphalt. Construction and Building Materials 53, 621-634.

Irons, J. R. and J. G. Masek (2006). Requirements for a landsat data continuity mission. Photogrammetric Engineering and Remote Sensing 72(10), 1102-1108.

Irons, J. R., J. L. Dwyer and J. A. Barsi (2012). The next landsat satellite: the landsat data continuity mission. Remote Sensing of Environment 122, 11-21.

Liu, Y., T. Fei, M. Bian and F. Corsi (2010). Assessment of underwater light climate for lake Dahuchi using field spectral data and landsat TM. International Journal of Remote Sensing 31(6),1625-1643.

Maglione, P., C. Parente and A. Vallario (2014). Coastline Extraction using high resolution worldview-2 satellite imagery. European Journal of Remote Sensing 47, 685-699.

Marcello, J., F. Eugenio, S. Estrada-Allis and P. Sangra (2015). Segmentation and tracking of anticyclonic eddies during a submarine volcanic eruption using ocean colour imagery. Sensors 15, 8732-8748.

Mumford, D. and J. Shah (1989). Optimal approximations by piecewise smooth functions and associated variational problems. Communication on Pure and Applied Mathematics 42(5), 577-685.

Osher, S. and J. A. Sethian (1988). Fronts propagating with curvature-dependent

speed: algorithms based on Hamilton-Jacobi formulations. Journal of Computational Physics 79(1), 12-49.

Pacheco, A., J. Horta, C. Loureiro and O. Ferreira (2015). Retrieval of nearshore bathymetry from landsat 8 images: a tool for coastal monitoring in shallow waters. Remote Sensing of Environment 159, 102-116.

Pahlevan, N., Z. Lee, J. Wei, C. B. Schaaf, J. R. Schott and A. Berk (2014). On-orbit radiometric characterization of OLI (Landsat-8) for applications in aquatic remote sensing. Remote Sensing of Environment 154, 272-284.

Palmer, S. C. J., P. D. Hunter, T. Lankester, S. Hubbard, E. Spyrakos, A. N. Tyler, M. Presing, H. Horvath, A. Lamb, H. Balzter and V. R. Toth (2015). Validation of envisat MERIS algorithms for chlorophyll retrieval in a large, turbid and optically-complex shallow lake. Remote Sensing of Environment 157, 158-169.

Reshitnyk, L., M. Costa, C. Robinson and P. Dearden (2014). Evaluation of worldview-2 and acoustic remote sensing for mapping benthic habitats in temperate coastal Pacific waters. Remote Sensing of Environment 153, 7-23.

Richards, J. A. (2013). Remote Sensing Digital Image Analysis, An Introduction, 5th edition, Springer-Verlag Berlin Heidelberg, 503.

Updike, T. and C. Comp (2010). Radiometric use of worldview-2 imagery. Digital Global Technical Notes, revision 1.0.

Vanhellemont, Q. and K. Ruddick (2015). Advantages of high quality SWIR bands for ocean colour processing: examples from landsat-8. Remote Sensing of Environment 161, 89-106.

Vese, L. A. and T. F. Chan (2002). A multiphase level set framework for image segmentation using the Mumford and Shah Model. International Journal of Computer 50(3), 271-293.

Wolf, A. F. (2010). Using WorldView 2 Vis-NIR MSI imagery to support land mapping and feature extraction using Normalized Difference Index Ratios. Proc. SPIE 2010, 8390.